Fraunhofer Institut
Techno- und
Wirtschaftsmathematik

I. Ginzburg, K. Steiner

Free surface Lattice-Boltzmann method to model the filling of expanding cavities by Bingham Fluids

Berichte des Fraunhofer ITWM, Nr. 28 (2001)

ISSN 1434-9973

Bericht 28 (2001)

Die Veröffentlichungen in der Berichtsreihe des Fraunhofer ITWM können bezogen werden über:

Fraunhofer-Institut für Techno- und
Wirtschaftsmathematik ITWM
Gottlieb-Daimler-Straße, Geb. 49

67663 Kaiserslautern

Telefon: +49 (0) 6 31/2 05-32 42
Telefax: +49 (0) 6 31/2 05-41 39
E-Mail: info@itwm.fhg.de
Internet: www.itwm.fhg.de

Vorwort

Das Tätigkeitsfeld des Fraunhofer Instituts für Techno- und Wirtschaftsmathematik ITWM umfasst anwendungsnahe Grundlagenforschung, angewandte Forschung sowie Beratung und kundenspezifische Lösungen auf allen Gebieten, die für Techno- und Wirtschaftsmathematik bedeutsam sind.

In der Reihe »Berichte des Fraunhofer ITWM« soll die Arbeit des Instituts kontinuierlich einer interessierten Öffentlichkeit in Industrie, Wirtschaft und Wissenschaft vorgestellt werden. Durch die enge Verzahnung mit dem Fachbereich Mathematik der Universität Kaiserslautern sowie durch zahlreiche Kooperationen mit internationalen Institutionen und Hochschulen in den Bereichen Ausbildung und Forschung ist ein großes Potenzial für Forschungsberichte vorhanden. In die Berichtreihe sollen sowohl hervorragende Diplom- und Projektarbeiten und Dissertationen als auch Forschungsberichte der Institutsmitarbeiter und Institutsgäste zu aktuellen Fragen der Techno- und Wirtschaftsmathematik aufgenommen werden.

Darüberhinaus bietet die Reihe ein Forum für die Berichterstattung über die zahlreichen Kooperationsprojekte des Instituts mit Partnern aus Industrie und Wirtschaft.

Berichterstattung heißt hier Dokumentation darüber, wie aktuelle Ergebnisse aus mathematischer Forschungs- und Entwicklungsarbeit in industrielle Anwendungen und Softwareprodukte transferiert werden, und wie umgekehrt Probleme der Praxis neue interessante mathematische Fragestellungen generieren.

Prof. Dr. Dieter Prätzel-Wolters
Institutsleiter

Kaiserslautern, im Juni 2001

Free surface lattice-Boltzmann method to model the filling of expanding cavities by Bingham Fluids.

By Irina Ginzburg and Konrad Steiner,

Fraunhofer Institut für Techno- und Wirtschaftsmathematik, Gottlieb-Daimler-Straße, Geb. 49, 67663 Kaiserslautern, Germany

accepted by the Phil. Trans. R. Soc. London, October 2001.

The filling process of viscoplastic metal alloys and plastics in expanding cavities is modelled using the lattice Boltzmann method in two and three dimensions. These models combine the regularized Bingham model for viscoplastic fluids with a free-interface algorithm. The latter is based on a modified immiscible lattice Boltzmann model in which one species is the fluid and the other one is considered as vacuum. The boundary conditions at the curved liquid-vacuum interface are met without any geometrical front reconstruction from a first-order Chapman-Enskog expansion. The numerical results obtained with these models are found in good agreement with available theoretical and numerical analysis.

Keywords: Generalized LBE; free-surface phenomena; interface boundary conditions; filling processes; Bingham viscoplastic model; regularized models.

1. Introduction

Two phase flow phenomena are ubiquitous in nature and in industrial applications. The filling of a die cavity in metal casting is such an example. In this case, the density ratio between the melt metal and the air is of such a disparity that the influence of the air on the melt metal can be ignored. The problem of two-fluid flow with an interface reduces then to the problem of one-fluid flow with free-boundary. The formulation of the free-boundary flow avoids the modelling of steep variations of physical quantities in the interfacial region. Several methods to treat the free-surface problem have been developed. Among volume tracking methods, the most popular one is the volume of fluid (VOF) method due to Hirt & Nicholls (1981). This method has been successfully applied to simulate mould filling with regular grids by Alexandrou *et al.* (2001), Bakhudarov *et al.* (1993). A review on free-surface methods for simulations in injection moulding is given by Kothe *et al.* (1998).

Dense suspensions of metal solid particles in liquid state (metal alloys) are used in manufacturing methods as well. Such materials behave as solids when the magnitude of the viscous stress is less than a yield stress. Above it, they behave as liquids with an effective (apparent) viscosity depending on the magnitude of the rate of strain. The behaviour of these viscoplastic fluids is well described by the Bingham model. A very interesting theoretical and numerical study of injection moulding in 2D cavity with Bingham fluids is found in Alexandrou *et al.* (2001).

In this paper, we present the construction of a viscoplastic model which couples the regularized Bingham model of Papanastasiou (1987) with the free interface lattice Boltzmann (LB) algorithm introduced by Ginzburg & Steiner (2001). Our approach to treat viscoplasticity is closer to the work of Aharonov & Rothman (1993) on viscoelastic fluids than to the LB modelling introduced by Giraud *et al.* (1997). The LB equation used here is based on the framework of the generalized lattice Boltzmann equation (GLBE) due to d'Humières (1992). The free surface algorithm is a modification of the Immiscible Lattice Boltzmann (ILB) model proposed by Gunstensen & Rothman (1992).

The paper is structured as follows. The regularized Bingham model and basic macroscopic two-phase relations are found in §2. In §3 the LB framework is given and the components of the strain rate tensor are locally obtained from the population distributions. In §4, the ILB method is reformulated to yield an algorithm which divides the memory requirement by almost a factor two. The free-interface LB algorithm is outlined in §5. The required first-order Chapman-Enskog expansion and reconstruction of the unknown populations at the interface are presented in §5 *c* and §5 *d* respectively. The model is applied to the filling of expanding cavities in §6. Concluding remarks are given in §7. Modelling surface tension with ILB models is discussed in the Appendix.

2. Hydrodynamics equations

(*a*) *Viscoplastic model*

In the context of athermal LB methods, the hydrodynamic equations for the density ρ and the momentum $\vec{j} = \rho\vec{u}$ are usually given in the following form:

$$\partial_t \rho + \nabla \cdot \vec{j} = 0 \,, \tag{2.1}$$

$$\partial_t \vec{j} + \nabla \cdot \left(\frac{\vec{j} \otimes \vec{j}}{\rho} \right) = -c_s^2 \nabla \rho + \nu \nabla \cdot (\nabla \vec{j}) + \nu_\xi \nabla (\nabla \cdot \vec{j}) + \vec{F} \,, \tag{2.2}$$

where $\vec{F}$ is the body force, ν and ν_ξ are respectively the kinematic and bulk viscosities, and the pressure P is given by the equation of state for an ideal gas,

$$P = c_s^2 \rho \,. \tag{2.3}$$

In Newtonian fluids the viscous stress tensor $\boldsymbol{\tau}$ is related to the rate of strain tensor $\mathsf{D} = (\nabla\vec{u} + (\nabla\vec{u})^t)/2$ by the linear relation $\boldsymbol{\tau} = 2\nu\mathsf{D}$. In viscoelastic or viscoplastic fluids this linear relation is no longer true and is replaced by so called 'constitutive equations'. One of them is the Bingham model for which the fluid behaves as a rigid solid when the norm of the viscous stress tensor $\boldsymbol{\tau}$ is less than a yield stress value τ_0. The so called 'yield surface' $\|\boldsymbol{\tau}\| = \tau_0$ separates two regions:

$$\begin{aligned} \|\mathsf{D}\| &= 0 \,, \qquad \text{if} \qquad \|\boldsymbol{\tau}\| < \tau_0 \,, \\ \boldsymbol{\tau} &= 2\left(\nu + \frac{\tau_0}{\|\mathsf{D}\|}\right)\mathsf{D} \,, \qquad \text{if} \qquad \|\boldsymbol{\tau}\| > \tau_0 \,, \end{aligned} \tag{2.4}$$

where $\|\mathsf{D}\| = \sqrt{2D_{ij}D_{ij}}$ and $\|\boldsymbol{\tau}\| = \sqrt{\tau_{ij}\tau_{ij}/2}$. When $\|\boldsymbol{\tau}\| > \tau_0$, the fluid has an effective viscosity ν^{eff}, $\nu^{\text{eff}} = \nu + \tau_0/\|\mathsf{D}\|$, with $\boldsymbol{\tau} = 2\nu^{\text{eff}}\mathsf{D}$. Numerical difficulties

come from the singularity at yield surface and we consider here the regularized model of Papanastasiou (1987) in a form

$$\boldsymbol{\tau} = 2\left[\nu + \frac{\tau_0(1-\exp\{-m\|\mathsf{D}\|\})}{\|\mathsf{D}\|}\right]\mathsf{D}\,. \tag{2.5}$$

Its applicability to predict viscoplastic behaviour in the limit $m \to \infty$ is studied by Burgos *et al.* (1999).

(*b*) *Non-dimensional two-phase equations*

In case of two immiscible fluids, say liquid-gas, equations (2.1) and (2.2) act in the bulk of each phase. Let ρ and ν (ρ^g and ν^g) refer to parameters of the liquid (gas) phase, accordingly. If the surface tension coefficient σ is constant, the surface tension force per unit area $\vec{F}_s$ acting on the interface S is defined as

$$\vec{F}_s = \sigma \vec{f}_s\,, \qquad \vec{f}_s = \kappa \vec{n} \delta_S\,, \tag{2.6}$$

where $\vec{n}(\vec{r})$ is the unit vector normal to S at $\vec{r}$, directed from the gas to the liquid, $\kappa(\vec{r}) = -(\nabla \cdot \vec{n})|_{\vec{r}}$ is the local curvature, taken positive if the centre of curvature is in the liquid phase, and δ_S is the Dirac distribution at the interface S.

Let us introduce characteristic length L and velocity U. Assuming density fluctuations around a bulk average value ρ_0 (ρ_0^g, respectively) and a force due to gravity ($\vec{F} = \rho_0 g \vec{1}_g$), the following scalings

$$x \to x/L\,,\ t \to tU/L\,,\ \vec{u} \to \vec{u}/U\,,\ P \to \frac{(P-P_0)}{\rho_0 U^2}\,,\ P_0 \equiv c_s^2 \rho_0\,,\ \vec{f}_s \to \vec{f}_s\, L^2\,. \tag{2.7}$$

yield the dimensionless one-phase hydrodynamic equations

$$\mathrm{M}^2 \partial_t P + \nabla \cdot \rho \vec{u} = 0\,, \qquad \rho = \rho_0\,(1 + \mathrm{M}^2 P\,), \tag{2.8}$$

$$\partial_t \rho \vec{u} + \nabla \cdot (\rho \vec{u} \otimes \vec{u}) = -\rho_0 \nabla P + \rho_0 \frac{\vec{1}_g}{\mathrm{Fr}} + \rho_0 \frac{\vec{f}_s}{\mathrm{We}} + \frac{1}{\mathrm{Re}} \frac{\nu^{\mathrm{eff.}}}{\nu} \nabla \cdot (\nabla \rho \vec{u}) + \nabla \left(\frac{\nu_\xi}{UL} \nabla \cdot (\rho \vec{u}) \right), \tag{2.9}$$

where Re, Fr, M, and We are respectively the Reynolds, Froude, Mach, and Weber numbers defined as

$$\mathrm{Re} = \frac{LU}{\nu}\,, \quad \mathrm{Fr} = \frac{U^2}{gL}\,, \quad \mathrm{M} = \frac{U}{c_s}\,, \quad \mathrm{We} = \frac{\rho_0 L U^2}{\sigma}\,. \tag{2.10}$$

An additional non-dimensional parameter, the Bingham number Bi, controls the viscoplastic effects (cf. equation (2.4)):

$$\mathrm{Bi} = \frac{\tau_0 L}{\nu U}\,,\ \mathsf{D}' = \frac{\mathsf{D}L}{U}\,,\ m' = \frac{mU}{L}\,,\ \frac{\nu^{\mathrm{eff.}}}{\nu} = 1 + \frac{\mathrm{Bi}(1-\exp\{-m'\|\mathsf{D}'\|\})}{\|\mathsf{D}'\|}\,. \tag{2.11}$$

If we choose to neglect the density fluctuations, which are second-order in Mach number as indicated in equation (2.8), we obtain the two-phase incompressible

Navier-Stokes equations as

$$\nabla \cdot \vec{u} = 0\,, \tag{2.12}$$

$$\partial_t \vec{u} + \vec{u} \cdot \nabla\, \vec{u} = \frac{\vec{1}_g}{\mathrm{Fr}} + \frac{1}{\rho'}\left[-\nabla P + \frac{1}{\mathrm{Re}}\frac{\nu^{\mathrm{eff}.}}{\nu}\nabla \cdot (2\rho'\nu'\mathsf{D}') + \frac{\vec{f}_s}{\mathrm{We}}\right], \tag{2.13}$$

where $\rho' = 1$ and $\nu' = 1$ in the liquid, and $\rho' = \rho_0^g/\rho_0$ and $\nu' = \nu^g/\nu$ in the gas.

(c) *Interface boundary conditions*

The velocity is assumed to be continuous across the interface S: $[\vec{u}]_S = 0$, where $[\psi]_S$ denotes the jump of ψ across S. Momentum conservation (2.13) supplies the additional interface jump condition (in dimensional variables)

$$[2\rho\nu\mathsf{D} \cdot \vec{n} - P\vec{n}]_S = \sigma \vec{f}_s\,. \tag{2.14}$$

When the dynamic viscosity ratio $\rho'\nu'$ is small enough to be neglected and if the surface tension and density fluctuations are also negligible, the above equation reduces to the following free-interface conditions for the heavy fluid (e.g. liquid)

$$P - 2\nu\frac{\partial j_n}{\partial n} = P_0\,, \tag{2.15}$$

$$\frac{\partial j_\tau}{\partial n} + \frac{\partial j_n}{\partial \tau} = 0\,. \tag{2.16}$$

Here j_n and $j_\tau = \{j_{\tau_1}, j_{\tau_2}\}$ are the normal and tangential ($\tau \in \{\tau_1, \tau_2\}$) momentum components of the viscous (heavy) fluid; and P and P_0 are respectively the pressures of the heavy and light fluids at the interface S.

3. Lattice Boltzmann framework

(a) *Lattice Boltzmann equation*

Following d'Humières (1992), we use lattice Boltzmann equation as its projection on an orthonormal basis in moment space

$$\tilde{N}_i(\vec{r}, t) = N_i(\vec{r}, t) + \sum_{k=0}^{b_m} \lambda_k(\mathbf{N} - \mathbf{N}^{\mathrm{eq}}, \mathbf{e}_k) e_{ki} \tag{3.1}$$

$$N_i(\vec{r} + \vec{C}_i, t+1) = \tilde{N}_i(\vec{r}, t)\,, \qquad i \in \{0, \ldots, b_m\}\,, \tag{3.2}$$

where N_i is the population of the particle moving with velocity $\vec{C}_i$ ($\vec{C}_0$ is a zero vector) and $\mathbf{N}^{\mathrm{eq}}$ is given in the following section. Equation (3.1) assumes that the basis vectors $\{\mathbf{e}_k\}$ represent the set of the eigenvectors of the collision matrix associated to the eigenvalues $\{\lambda_k\}$. The basis vectors can be found in d'Humières (1992) and Lallemand & Luo (2000) for the nine-velocity model in two dimensions ($D2Q9$) and in d'Humières *et al.* (2001) for the fifteen-velocity model in three dimensions ($D3Q15$). These basis are referred below as *the general moment basis*.

(*b*) *Equilibrium function*

When a forcing term $\vec{F}$ is present, density ρ and momentum $\vec{j}$ are defined as

$$\rho(\vec{r},t) = \sum_{i=0}^{b_m} N_i(\vec{r},t) \ , \quad \vec{j}(\vec{r},t) = \vec{J} + \frac{1}{2}\vec{F} \ , \quad \vec{J} = \sum_{i=1}^{b_m} N_i(\vec{r},t)\vec{C}_i \ . \tag{3.3}$$

The reason to use the above momentum definition is discussed by Ginzbourg & Adler (1994) and Buick & Greated (2000).

From the set of possible equilibrium distributions leading to the Navier-Stokes equations, we use here the following function

$$N_i^{\rm eq} = t_p^\star \left[c_s^2\rho + J_\alpha C_{i\alpha} + \frac{j_\alpha j_\beta}{2\rho}(3C_{i\alpha}C_{i\beta} - \delta_{\alpha\beta}) \right] , \tag{3.4}$$

where the index p is equal to c_i^2 ($c_i^2 = \|\vec{C}_i\|^2$) and the parameters $t_p^\star$ are:
$t_0^\star c_s^2 = 1 - 5c_s^2/3$, $t_1^\star = 1/3$, $t_2^\star = 1/12$ for $D2Q9$ and
$t_0^\star c_s^2 = 1 - 7c_s^2/3$, $t_1^\star = 1/3$, $t_3^\star = 1/24$ for $D3Q15$.
The speed of sound c_s (cf. equation (2.3)) is chosen such that $c_s^2 = 1/3$, an optimal choice according to Lallemand & Luo (2000). The body force $\vec{F}$ is obtained by adding the quantity $t_p^\star \vec{C}_i \cdot \vec{F}$ to $\tilde{N}_i(\vec{r},t)$ in equation (3.1).

(*c*) *First-order correction to equilibrium*

Following Frisch *et al.* (1987), the solution for the population function N_i can be obtained from a Chapman-Enskog expansion in powers of a small perturbation parameter $\epsilon = \delta_x/L$:

$$N_i(\vec{r},t) = N_i^{\rm eq}(\vec{r},t) + \epsilon N_i^{(1)}(\vec{r},t) + \epsilon^2 N_i^{(2)}(\vec{r},t) + O(\epsilon^3) \ , \ i = 0, \ldots, b_m \ . \tag{3.5}$$

For the free-interface algorithm, one crucial ingredient is that $\epsilon\mathbf{N}^{(1)}$ is isotropic (rotational invariant), thus is given in any orthogonal coordinate system $\{x', y', z'\}$ (z' is omitted in two dimensions, see Ginzburg & Steiner 2001 for details) by:

$$\epsilon N_i^{(1)} = \frac{1}{\lambda_\psi}\frac{\partial j_{\alpha'}}{\partial \beta'} Q_{i\alpha'\beta'} + \frac{1}{\lambda_e}(\nabla\cdot\vec{j})E_i^{\rm im} \ , \quad \{\alpha', \beta'\} \in \{x', y', z'\} \ . \tag{3.6}$$

$$Q_{i\alpha'\beta'} = t_p^\star \left(C_{i\alpha'}C_{i\beta'} - \frac{c_i^2}{D}\delta_{\alpha'\beta'} \right) , \quad E_i^{\rm im} = t_p^\star \left(\frac{c_i^2}{D} - c_s^2 \right) . \tag{3.7}$$

In the standard coordinate system $(x', y', z') = (x, y, z)$, the terms $Q_{i\alpha'\beta'}$ are linear combinations of the components of eigenvectors defined in the general moment basis (d'Humières *et al.* 2001). These eigenvectors are those associated to the viscous stress tensor and λ_ψ is the corresponding eigenvalue. $\mathbf{E}^{\rm im}$ is a linear combination of the two eigenvectors corresponding to energy and energy square in the same basis and has the eigenvalue λ_e. Kinematic and bulk viscosities, ν and ν_ξ respectively, are related to λ_ψ and λ_e by

$$\nu = -\frac{1}{3}\left(\frac{1}{\lambda_\psi} + \frac{1}{2}\right) , \quad \nu_\xi = \frac{D-2}{D}\nu - \left(\frac{D+2}{3D} - c_s^2\right)\left(\frac{1}{\lambda_e} + \frac{1}{2}\right) . \tag{3.8}$$

The above eigenvalues can be easily adjusted during computation as required for two phase models or to account for viscoelastic or viscoplastic effects. Note that these eigenvalues must stay in the interval $]-2, 0[$ for linear stability.

(d) Local computations of the stress tensor

In the coordinate system $(x', y', z') = (x, y, z)$, the components of strain rate tensor D^{j}, $\mathsf{D}^{\mathsf{j}} = (\nabla\vec{j} + (\nabla\vec{j})^t)/2$, can be computed with an $O(\epsilon^2)$ error from the non-equilibrium projection b_k on the basis vectors $\mathbf{e}_k$:

$$b_k = \lambda_k \frac{(\mathbf{N} - \mathbf{N}^{\mathrm{eq}}, \mathbf{e}_k)}{\| \mathbf{e}_k \|^2} ,$$

$$\frac{\partial j_x}{\partial y} + \frac{\partial j_y}{\partial x} = b_1 , \qquad \frac{\partial j_x}{\partial x} - \frac{\partial j_y}{\partial y} = b_2 , \qquad \frac{\partial j_x}{\partial x} + \frac{\partial j_y}{\partial y} = b_3 ,$$

$$\mathbf{e}_1 = \{t_p^\star C_{ix} C_{iy}\} , \quad \mathbf{e}_2 = \{t_p^\star (C_{ix}^2 - c_i^2/2)\} , \quad \mathbf{e}_3 = \{E_i^{\mathrm{im}}\} , \tag{3.9}$$

in two dimensions, and

$$\frac{\partial j_x}{\partial x} - \frac{1}{2}\left(\frac{\partial j_y}{\partial y} + \frac{\partial j_z}{\partial z}\right) = b_1 , \quad \frac{1}{2}\left(\frac{\partial j_y}{\partial y} - \frac{\partial j_z}{\partial z}\right) = b_2 , \quad \frac{\partial j_x}{\partial x} + \frac{\partial j_y}{\partial y} + \frac{\partial j_z}{\partial z} = b_3 ,$$

$$\frac{\partial j_x}{\partial y} + \frac{\partial j_y}{\partial x} = b_4 , \qquad \frac{\partial j_x}{\partial z} + \frac{\partial j_z}{\partial x} = b_5 , \qquad \frac{\partial j_y}{\partial z} + \frac{\partial j_z}{\partial y} = b_6 ,$$

$$\mathbf{e}_1 = \{t_p^\star (C_{ix}^2 - c_i^2/3)\} , \quad \mathbf{e}_2 = \{t_p^\star (C_{iy}^2 - C_{iz}^2)\} , \quad \mathbf{e}_3 = \{E_i^{\mathrm{im}}\} ,$$

$$\mathbf{e}_4 = \{t_p^\star C_{ix} C_{iy}\} , \quad \mathbf{e}_5 = \{t_p^\star C_{ix} C_{iz}\} , \quad \mathbf{e}_6 = \{t_p^\star C_{iy} C_{iz}\} , \tag{3.10}$$

in three dimensions. Note that some of the above results are derived from relations (3.7) using $\sum_{\alpha'} Q_{i\alpha'\alpha'} = 0$. When incompressible flow is assumed, b_3 can be set to zero, simplifying the above relations for the diagonal components of the stress tensor. The magnitude of the strain rate tensor $\|\mathsf{D}\|$ is estimated from the relations (3.9) and (3.10), where λ_ψ is derived from the local value of $\nu^{\mathrm{eff}\cdot}$ at the previous time step using relation (3.8). Then the new value of $\nu^{\mathrm{eff}\cdot}(t)$ is computed according to relation (2.5). If $\|\boldsymbol{\tau}\| < \tau_0$, $\nu^{\mathrm{eff}\cdot}(t)$ is set equal to its limit value $\nu + \tau_0 m$.

4. Two-phase lattice Boltzmann model

(a) Reformulated ILB model

One early Lattice Boltzmann model for immiscible fluids has been proposed by Gunstensen & Rothman (1992) and was originally designed to simulate flows of two immiscible fluids differentiated only by their colours. In order to describe the two fluids, the original model uses two kinds of populations: $\{R_i(\vec{r}, t)\}$ and $\{B_i(\vec{r}, t)\}$, but operates only on their sums. Thus it is equivalent to use as independent variables of the model only one kind of populations, say $N_i(\vec{r}, t)$, and the total density of one fluid $\rho_f(\vec{r}, t)$:

$$N_i(\vec{r}, t) = R_i(\vec{r}, t) + B_i(\vec{r}, t) , \qquad \rho_f(\vec{r}, t) = \sum_{i=0}^{b_m} R_i(\vec{r}, t) . \tag{4.1}$$

The local density of the other fluid is then equal to $\rho(\vec{r}, t) - \rho_f(\vec{r}, t)$.

In addition to the usual collision and advection steps, the ILB model has a "recolouring" step, which preferentially redirects each fluid to the neighbouring sites of the same colour in order to keep a sharp front. For this we use a similar

but slightly different method. The vector $\vec{n}$ normal to the interface, $\vec{n} \approx \nabla\rho_f$, is estimated by using the following central difference stencil

$$s = \begin{cases} 1/4 \times \{2,2,2,2,1,1,1,1\}\,, & \text{for } D2Q9\ , \\ 1/8 \times \{4,4,4,4,4,4,1,1,1,1,1,1,1,1\}\,, & \text{for } D3Q15\ , \end{cases}$$

and the following approximation

$$\vec{n} = \sum_{i=1}^{b_m} s_i \vec{C}_i \frac{\rho_f(\vec{r}+\vec{C}_i)}{\rho(\vec{r}+\vec{C}_i)}\ , \tag{4.2}$$

Then one has to find the solution $\mathbf{N}^{\mathrm{R}}(\vec{r},t)$ which maximizes the post-collision fluid flux $\tilde{F}[\mathbf{R}]$ along the normal $\vec{n}$ to the interface:

$$\tilde{F}(\mathbf{R}) = \sum_{i=0}^{b_m} R_i\ \vec{C}_i \cdot \vec{n}\ , \quad \sum_{i=0}^{b_m} R_i = \rho_f(\vec{r},t)\ , \quad 0 \le R_i \le \tilde{N}_i(\vec{r},t)\ . \tag{4.3}$$

The solution is constrained by mass conservation. Note that the above inequality imposes the post-collision populations to be positive. The way we treat the negative populations is described in §5 *d*. The new value $\rho_f(\vec{r},t+1)$ is equal to the sum of all incoming fluid quantities $N_i^R(\vec{r}-\vec{C}_i,t)$:

$$\rho_f(\vec{r},t+1) = \sum_{i=0}^{b_m} N_i^R(\vec{r}-\vec{C}_i,t)\ . \tag{4.4}$$

Since $\rho_f(\vec{r},t+1)$ can be updated immediately after recolouring steps in neighbouring nodes, no additional storage is needed for the solution $\mathbf{N}^{\mathrm{R}}(\vec{r},t)$ and this algorithm reduces the ILB memory requirement by a factor two.

Wetting/non-wetting conditions at solid boundary are controlled by setting $\rho_f(\vec{r}_{\mathrm{solid}}) = \rho_f \times w$, with $w > 0$ for wetting cases and $w \le 0$ otherwise.

(*b*) *Outline of the two-phase algorithm*

We initialize first ρ_f and $\{N_i(\vec{r},t)\}$ in all cells at $t = 0$. Interfacial cells are those where $0 < \rho_f < \rho$. Subsequent steps at time t, $t = 0, \ldots,$ are:

1. Compute the normal $\vec{n}(\vec{r},t)$ to the interface.
2. Perform LB equation and put $\rho_f(\vec{r},t+1)$ equal to zero in all cells.
3. Update $\rho_f(\vec{r},t+1)$ by the recolouring technique (equation (4.4)).
4. Propagate the populations.
5. $t = t+1$; Go to **1**.

5. Lattice Boltzmann model for free-interface

(a) *Main ideas*

The LB method for free-interface is based on the ILB model described in the previous section. The fundamental difference between the two approaches is that only one of the two phases is considered as an actual fluid in the free-interface model. Then the part of the algorithm corresponding to equation (3.1) applies only to the cells which are fully or partially filled with this fluid ($\rho_f > 0$). The second key ingredient is the reconstruction step of the populations which are not coming from the fluid at the interface cells. This step follows the basic philosophy of the local second-order boundary (LSOB) method of Ginzbourg & d'Humières (1996) where all the first- and second-order momentum derivatives, necessary to impose Dirichlet boundary conditions, are extracted from locally known populations. Here the unknown macroscopic quantities at the interface cells (density and momentum in 2D, plus two combinations of the tangential derivatives of the momentum in 3D) are extracted locally as solutions of a linear system built from the known populations arriving from the fluid. This system comes from enforcing the exact boundary conditions at the curved gas-liquid interface in a first-order Chapman-Enskog expansion (3.6) written in the local coordinates, normal and tangent to the free-surface. The solution of the linearized system is then used in the expansion to compute the unknown populations. Finally a recolouring step, similar to that in the ILB models, is used to keep a sharp moving front.

(b) *Outline of the free-surface algorithm*

Similar as in two phase algorithm, the populations $\{N_i(\vec{r},t)\}$ and the mass fraction of fluid $\rho_f(\vec{r},t)$ represent the main independent variables of the LB free-surface algorithm. In empty cells, $\rho_f = 0$; in the cells fully filled with fluid, $\rho_f = \rho$ and in partially filled cells, $0 < \rho_f < \rho$. We initialize first ρ_f in all liquid cells at $t = 0$. The populations are then initialized to their equilibrium values, and a first collision step is performed in active cells where $\rho_f > 0$. We refer below to active cells as $A(t)-$cells. Subsequent steps at time t, $t = 0, \ldots,$ are:

1. Compute $\rho_f(\vec{r}, t+1)$ in all cells by recolouring technique.
2. Divide all cells into active/non-active cells:
   $(\vec{r}, t+1) \in A(t+1)$ if $\rho_f(\vec{r}, t+1) > 0$; otherwise it is non-active.
3. Propagate populations from $A(t)$ into $A(t+1)$ cells.
4. Classify known/unknown populations in $A(t+1)$ cells: $N_i(\vec{r}, t+1)$ is marked as *known population* if $(\vec{r} - \vec{C}_i, t) \in A(t)$. Otherwise it is marked as *unknown population.*
5. Divide $A(t+1)$ cells into B/I/N-cells:
   - $(\vec{r}, t+1)$ is marked as B(*bulk*)-cell if it contains only known populations.
   - $(\vec{r}, t+1)$ is marked as I(*interface*)-cell if it has at least one unknown population and if $(\vec{r}, t) \in A(t)$.

- $(\vec{r}, t+1)$ is marked as N(*new interface*)-cell otherwise.

6. Perform collision in B-cells.
7. Perform reconstruction and collision in I-cells.
8. Perform reconstruction and collision in N-cells.
9. $t = t+1$; Go to **1**.

This completes the short description of the LB free-interface algorithm. The specific steps of the algorithm are given in the next sections and more details can be found in Ginzburg & Steiner (2001).

(*c*) *First-order expansion of N_i at the interface*

The unknown populations at the interface are constructed by using the first-order approximation (3.6) written in local coordinates, normal and tangent to the free-surface: $(x', y', z') = (n, \tau_1, \tau_2)$. Since surface tension is not included into our current free surface algorithm, the non-diagonal components of the strain-rate tensor are prefactors of $\mathbf{Q}_{n\tau}$ ($\mathbf{Q}_{n\tau_1}$, $\mathbf{Q}_{n\tau_2}$) in equation (3.5) and are set to zero at the interface according to the boundary condition (2.16). Since $\nabla\cdot\vec{j}$ is of order $O(\mathrm{M}^2)$, it can be neglected for incompressible flows. Then using the boundary condition (2.15) for $\partial j_n/\partial n$ and the continuity relation, equation (3.5) becomes

$$N_i = N_i^{\mathrm{eq}} + \frac{(P-P_0)}{\nu\,\lambda_\psi} Q_{inn} + O(\epsilon^2)\,, \tag{5.1}$$

in two-dimensions, and

$$\begin{aligned} N_i \;=\; & N_i^{\mathrm{eq}} + \frac{3(P-P_0)}{4\lambda_\psi\nu} Q_{inn} + \frac{1}{2\lambda_\psi}(Q_{i\tau_1\tau_1} - Q_{i\tau_2\tau_2})\left(\frac{\partial j_{\tau_1}}{\partial\tau_1} - \frac{\partial j_{\tau_2}}{\partial\tau_2}\right) \\ & + \frac{1}{\lambda_\psi} Q_{i\tau_1\tau_2}\left(\frac{\partial j_{\tau_1}}{\partial\tau_2} + \frac{\partial j_{\tau_2}}{\partial\tau_1}\right) + O(\epsilon^2)\,, \end{aligned} \tag{5.2}$$

in three dimensions (see also the derivation of relations (3.9) and (3.10)). The reconstruction step described in the next section assumes a linear approximation of the above relations with respect to the macroscopic quantities. The required linearization of the non-linear part of the equilibrium function can be done with respect to either momentum or density as

$$\rho u_\alpha u_\beta \approx j_\alpha u^\star_\beta\,, \quad \text{or} \quad \rho u_\alpha u_\beta \approx \rho u^\star_\alpha u^\star_\beta\,. \tag{5.3}$$

So far the actual choice does not seem to change the numerical properties of the model. The approximate values $\rho^\star$ and $\vec{u}^\star$ (and $\lambda^\star_\psi(\nu^{\mathrm{eff}}\cdot)$ for viscoplastic models) are obtained as follows. In already active I-cells, the solution at previous time step is used. In new interface N-cells, an extrapolation from the closest active cell along the normal $\vec{n}$ is used. By definition a N-cell has always at least one active neighbour, otherwise it would not have been activated. Since the collision, and hence the update of ρ and $\vec{u}$, is done first in B- and I-cells, the reconstruction step in N-cells can use current values in 'good' neighbours for extrapolations (see the steps **6**, **7**, **8** of the algorithm above). Additionally, other successful N-cells can be used for extrapolations.

(*d*) *Reconstruction step.*

According to the algorithm sketched in §5 *b*, a cell is active if its ρ_f value is positive and it is an interface active cell if its populations are split into two non-empty sets: known populations arriving from already active cells and unknown populations which would arrive from non-active cells. Let us denote with I^+ (I^-) the set of indices of locally known (unknown) populations N_i^+ (N_i^-, respectively). The numbers s^+ and s^- of known and unknown populations are related by

$$s^+ + s^- = b_m + 1 \ . \tag{5.4}$$

After the equilibrium function has been linearized, the population expansions (5.1) or (5.2) are linear functions of the components of the following vector $\vec{X}$:

$$\vec{X} = \begin{cases} \{\rho, j_x, j_y\} \ , & \text{in 2D} \\ \left\{\rho, j_x, j_y, j_z, \dfrac{\partial j_{\tau_1}}{\partial \tau_1} - \dfrac{\partial j_{\tau_2}}{\partial \tau_2}, \dfrac{\partial j_{\tau_1}}{\partial \tau_2} + \dfrac{\partial j_{\tau_2}}{\partial \tau_1}\right\}, & \text{in 3D} \ , \end{cases} \tag{5.5}$$

which contains $n_v = 3$ unknown macroscopic quantities in $2D$ and $n_v = 6$ unknowns in $3D$ (if the term $\nabla \cdot \vec{j}$ is not neglected in equation (3.7), it is included into the list of variables $\vec{X}$). A further constraint (approximate density definition) on $\vec{X}$ considerably improves stability and accuracy:

$$\rho - \sum_{i \in I^-} N_i^- = \sum_{i \in I^+} N_i^+ \ , \tag{5.6}$$

where the N_i^-'s are expressed as linear functions of $\vec{X}$.

The equations to find $\vec{X}$ are the s^+ linearized distribution functions for the known populations N_i^+ and the above constraint, i.e. $m = s^+ + 1$ equations with $2 \leq m \leq b_m + 1$. The number of variables n_v is equal to the number of components of the vector $\vec{X}$. When $n_v \leq m$, we solve the linear system by using fast least-square method with permutations. The unknown populations are then reconstructed from relations (5.1) or (5.2). If the linear solver detects a singular system, or if $n_v > m$, the unknown populations are extrapolated from active neighbours. A similar procedure is employed when negative populations appear after reconstruction or collision steps. Ginzburg & Steiner (2001) show that the relative part of such 'bad' situations is very small for stable calculations.

6. Numerical results

We show some first results obtained in injection moulding with Bingham fluids. Ginzburg & Steiner (2001) stress that relatively small values for LB inlet velocities have to be used in filling simulations at small Reynolds numbers in order to maintain reasonable values of the LB kinematic viscosity. Otherwise, inaccuracy of first-order Chapman-Enskog approximation and/or boundary conditions for high LB viscosities ($\nu > 1$) can lead to unsatisfactory results. In the present study, the boundary conditions at fluid-solid interfaces are realized by using combinations of the bounce-back and local specular reflection schemes. It is well known that the effective accuracy of bounce-back scheme deteriorates drastically when ν increases.

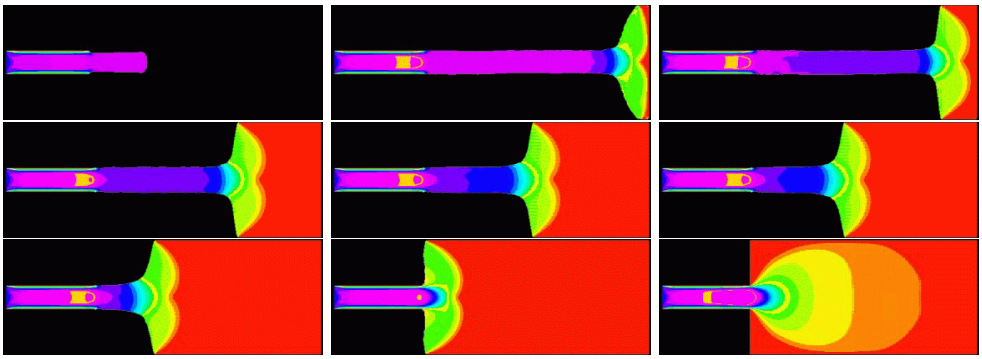

Figure 1. Velocity magnitude in 2D cavity at Re = 50, Bi = 10, $m' = 200$: (from left to right and from top to bottom, t [s] = 0.11, 0.27, 0.32, 0.43, 0.54, 0.59, 0.75, 0.92, and 1.02). The number of cells is 86240. LB data: $U^{lb} = 0.1$, $\nu^{lb} = 0.08$, $L^{lb} = 40$, $T^{lb} = 21560$. No-slip boundary conditions. Colours [cm/s]: red $(0-15)$, yellow $(15-25)$, green $(25-55)$, blue $(60-115)$, violet (>115).

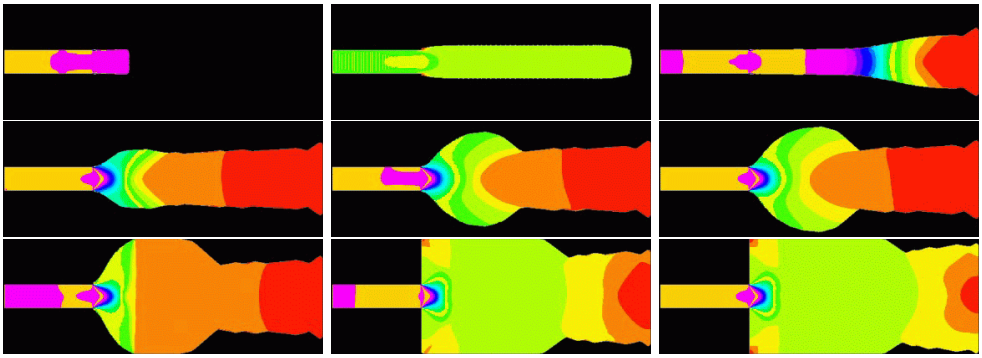

Figure 2. Velocity magnitude in 2D cavity at Re= 12.5, $Bi = 9.4$, $m' = 50$, $U^{lb} = 0.025$, $T^{lb} = 86240$. Free-slip boundary conditions. Other parameters are the same as in figure 1. Colours [cm/s]: red $(0-15)$, yellow $(15-25)$, green $(25-55)$, blue $(55-90)$, violet (>90).

The location of solid walls can be improved, however, when some eigenvalues of the collision matrix are related to the kinematic viscosity according to Ginzbourg & Adler (1994). These eigenvalues are associated to the odd order polynomial vectors in the general moment basis. For bounce-back condition, they are set to the value leading to an exact solution for plane Poiseuille flow. They are set to -1 for free-slip boundary conditions. Based on the results of Lallemand & Luo (2000), the eigenvalue λ_e is usually set to -1 (cf. relations (3.7)) in order to reduce the effects of the compression mode on stability.

We consider first filling simulations in a 2D cavity with expansion 1 : 5. The inlet section is 2 cm$\times$7.8 cm and the cavity is 10 cm$\times$20 cm; the inlet velocity is equal to 100 cm/s and the filling time T is 1.08 s. The characteristic length L is set equal to 2 cm. Gravitation is absent: $\vec{g} = 0$, the fluid density ρ_0 is 1 g/cm^3, and the linearization of the equilibrium function is done with respect to density (second relation 5.3). Simulations without viscoplastic effects for Re = 0.2, 2, 50, 500 can be found in Ginzburg & Steiner (2001). As a whole, the filling patterns are in good

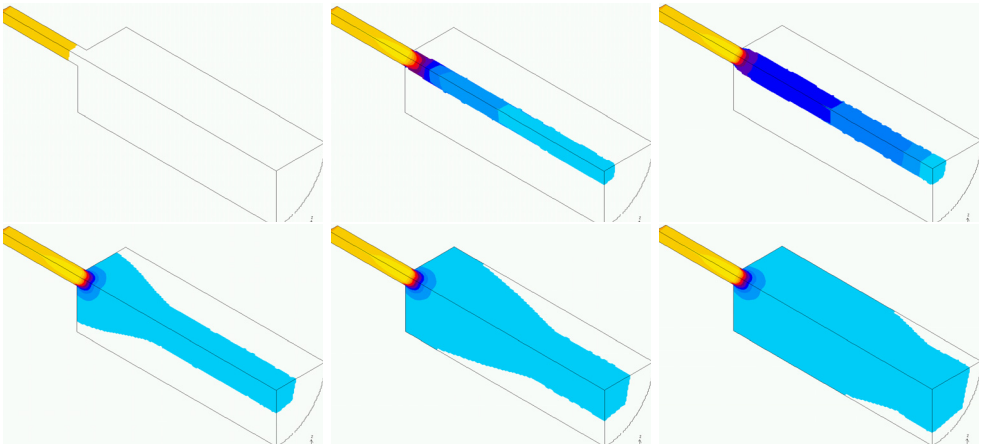

Figure 3. Velocity magnitude in a quarter of cylinder at Re = 12.5, Bi = 9.4, $m' = 50$: t [s] = 0.07, 0.43, 0.58, 1.73, 2.01, and 5.75. Grid: 385426 liquid cells. LB: $U^{lb} = 0.025$, $\nu^{lb} = 0.04$, $L^{lb} = 20$, $T^{lb} = 230105$. Free slip boundary conditions at all boundaries. Colours [cm/s]: blue $(0 - 32)$, red $(54 - 75)$, yellow (> 107).

agreement with the theoretical and the numerical analysis of Alexandrou *et al.* (2001). The results given in figure 1 show the viscoplastic behaviour at Re = 50, Bi = 10, using $m' = 200$. The obtained 'disk' filling patterns agree very well with the prediction of Alexandrou *et al.* (2001). The simulations in 2D cavity at Re = 12.5, Bi = 9.4, $m' = 50$ (figure 2) correspond to the transition from 'disk' to 'bubble' filling patterns which is typical for this range of Re and Bi values. In agreement to predictions of Burgos *et al.* (1999), further increase of the regularized parameter does not influence much the results. When free slip boundary conditions are used, some differences in the spreading behaviour can be observed near the stagnation point compared to the results of Alexandrou *et al.* (2001).

The last experiment has been repeated in 3D, by using a cylinder whose characteristic sizes are equal to those of a 2D cavity. The inlet section is 2 cm in diameter and 7.8 cm long; the cavity is 10 cm in diameter and 20 cm long; the inlet velocity is equal to 100 cm/s and the filling time T is 5.75 s. The linearization of the equilibrium function is done with respect to momentum (first relation 5.3) The results are shown in figure 3. Similar to the 2D case, the solution corresponds to an intermediate stage between mound and bubble regimes which could not be reproduced without accounting for the yield stress.

7. Concluding remarks

Free surface model of Ginzburg & Steiner (2001) is coupled to the regularized Bingham model in a simple and explicit in time manner. The method needs further investigation for strong viscoplastic regimes where iterative improvement of the effective viscosity approximation may become necessary in collision and/or reconstruction steps. Efficient and robust free-interface computations at very low Reynolds numbers require to find a way to maintain accuracy at high viscosity values. Although the problem can be avoided by restricting the LB viscosities to their reliable interval, the corresponding reduction in LB velocities slows down the

method. Despite these difficulties, the method seems very promising for modelling more general constitutive laws of Herschel-Bulkley fluids in free-interface and multiphase simulations.

This work has been partially financed by the DFG Project 'Die verallgemeinerte Lattice Boltzmann Methode für freie Randwertprobleme und Mehrphasenströmungen'. The authors are grateful to P. Klein, M. Beck, D. d'Humières, P. Lallemand, J. Linn, M. D. Lipinski, C. Lojewski, F. J. Pfreundt, D. Reinel-Bitzer and W. Schäfer for useful discussions and help.

Appendix A. Modelling surface tension in ILB

In ILB models the surface tension is created by a perturbation $\delta N^\sigma(\vec{r},t)$ of the populations $\tilde{N}_i(\vec{r},t)$, with

$$\delta N^\sigma(\vec{r},t) = A \parallel \vec{n} \parallel Q_{inn} , \qquad Q_{inn} = t_p^\star \left(C_{in}^2 - \frac{c_i^2}{D} \right) , \tag{A 1}$$

where A is a constant. Note that δN^σ in (A 1) is isotropic with respect to the interface orientation, unlike the perturbation term given in Nie *et al.* (1998). Assuming a flat interface perpendicular to a direction z along one of the main axes of the lattice, the stationary solution of the LB equation has the form:

$$N_i(z) = t_p^\star c_s^2 p(z) - \frac{1}{\lambda_\psi} A \parallel \vec{n} \parallel Q_{inn} + O(\epsilon^2) , \tag{A 2}$$

and the surface tension can be obtained from its mechanical definition as

$$\sigma \approx -\frac{2A}{3} \int_{-\infty}^{\infty} \frac{1}{\lambda_\psi} \|\vec{n}\| dz \approx \left\{ \begin{array}{ll} 8A(\nu + \nu^g + 1/3) & \text{for } D2Q9 \\ 16A(\nu + \nu^g + 1/3) & \text{for } D3Q15 \end{array} \right\} . \tag{A 3}$$

The error made in approximation (A 3) when the kinematic viscosities are different can be very important for large differences. However its leading order term vanishes if the interface value $\nu^{\text{int.}}(z_{\text{int.}})$ is:

$$\nu^{\text{int.}} = \rho_f(z_{\text{int.}})\nu + (1 - \rho_f(z_{\text{int.}}))\nu^g . \tag{A 4}$$

Laplace law and a numerical study done in realistic two phase (oil-gas) simulations in fibre materials (Ginzburg & Reinel-Bitzer 1999) confirm this result.

Note that for $\rho_f(z_{\text{int.}}) = 1/2$, the interface value of $\lambda_\psi^{\text{int.}}$ in equation (A 4) is equal to the harmonic mean of the eigenvalues λ_ψ and λ_ψ^g. This result is in apparent contradiction with an exact solution obtained by Ginzbourg & Adler (1995) for Poiseuille flow with a flat interface between the two phases. In this exact solution the interface viscosity has to be equal to the harmonic mean of the bulk values.

Owing to the problem at the interface mentioned above, the ILB model has difficulty to deal with large dynamic viscosity ratio. In addition, the effective interface boundary conditions implicitly imposed by the LB multi-phase methods have not yet received sufficient attention. For instance, assuming that $\delta_S \approx \|\nabla(\rho_f/\rho)\|$ does not change in the direction normal to the interface, Lafaurie *et al.* (1995) have shown for their VOF scheme that $\vec{F}_s$ is included into equation (2.2) as

$$\vec{F}_s \approx -\sigma \, \nabla \cdot \mathbf{T} , \qquad \mathbf{T} = (\mathbf{I} - \vec{n} \otimes \vec{n})\delta_S . \tag{A 5}$$

From momentum conservation, it can be shown that a similar result holds for ILB models using the population perturbation (A 1). The momentum conserving form (A 5) is usually associated to the 'spurious' currents observed for curved interfaces.

References

Alexandrou, A. N., Duc, E. & Entov, V. 2001 Inertial, viscous and yield stress effects in Bingham fluid filling of a 2-D cavity. *J. of Non-Newtonian Fluid Mech.* **96**, 383–403.

Aharonov, E. & Rothman, D. H. 1993 Non-Newtonian flow (through porous media): a lattice-Boltzmann method. *Geophys. Res. Lett.* **20**, 679–682.

Bakhudarov, M., You, H., Ortega, J., Beech, J., Chin, S. B. & Kirkwood, D. H. 1993 Experimental validation & development of FLOW-3D for casting problems. In *Modeling of Casting Welding and Advanced Solidification Processes-VI*, Proc. VI th. Int. Conf. 1993, Palm Beach, FL, TMS, AIME, pp. 421–434.

Buick, J. M. & Greated, C. A. 2000 Gravity in a lattice Boltzmann model. *Phys. Rev.* E **61**, 5307–5319.

Burgos, G. R., Alexandrou, A. N. & Entov, V. 1999 On the determination of yield surfaces in Herschel-Bulkley fluids. *J. of Rheol.* **43**, 463–483.

Frisch, U., d'Humières, D., Hasslacher, B., Lallemand, P., Pomeau, Y. & Rivet, J.-P. 1987, Lattice gas hydrodynamics in two and three dimensions. *Complex Sys.* **1**, 649-707.

Ginzbourg, I. & Adler, P. M. 1994 Boundary flow condition analysis for three-dimensional lattice Boltzmann model. *J. Phys. II France* **4**, 191–214.

Ginzbourg, I. & Adler, P. M. 1995 Surface tension models with different viscosities. *Transport in Porous Media* **20**, 37-76.

Ginzbourg, I. & d'Humières, D. 1996 Local second-order boundary method for lattice Boltzmann models. *J. Stat. Phys.* **84**, 927-971.

Ginzburg, I. & Reinel-Bitzer, D. 1999, Annual Report §3.6, ITWM, Kaiserslautern, `http://www.itwm.fhg.de/zentral/pdf/ar99_complete.pdf` .

Ginzburg, I. 2001 Introduction of upwind and free boundary into lattice Boltzmann method. In *Discrete Modelling and Discrete Algorithms in Continuum Mechanics* (eds T. Sonar & I. Thomas). Berlin: Logos-Verl, pp. 97–110.

Ginzburg, I. & Steiner, K. 2001 Lattice Boltzmann model for free-surface and its application to filling process in casting. Submitted to *J. Comp. Phys.* .

Giraud, L., d'Humières, D. & Lallemand, P. 1997 A lattice Boltzmann model for viscoelasticity. *Int. J. Mod. Phys. C.* **8**, 805–815.

Gunstensen, A. K. & Rothman, D. H. 1992 Microscopic modeling of immiscible fluids in three dimensions by a lattice-Boltzmann method. *Europhys. Lett.* **18**, 157–161.

Hirt, C. W. & Nicholls, B. D. 1981 Volume of fluid (VOF) method for the dynamics of free boundaries. *J. Comp. Phys.* **39**, 201–225.

d'Humières, D. 1992 Generalized lattice-Boltzmann equations. In *Rarefied Gas Dynamics: Theory and Simulations*, (eds B. D. Shizgal & D. P. Weaver), Progress in Astronautics and Aeronautics, vol. **159**, pp. 450–458. AIAA.

d'Humières, D., Ginzburg, I., Krafczyk, M., Lallemand, P. & Luo, L.-S. 2001 Multi-time relaxation lattice Boltzmann model in three dimensions. These Proceedings.

Kothe, D., Juric, D., Lam, K. & Lally, B. 1998 Numerical recipes for mold filling simulation. In *Modeling of casting welding and advanced solidification* (eds B. G. Thomas & C. Beckermann), The Minerals, Metals and Materials Society, pp. 17–28.

Lafaurie, B., Nardone, C., Scardovelli, R. & Zaleski, S. 1994 Modeling merging & fragmentation in multiphase flows with SURFER. *J. Comp. Phys.* **112**, 134–148.

Lallemand, P. & Luo, L.-S. 2000 Theory of the lattice Boltzmann method: dispersion, dissipation, isotropy, Galilean invariance, and stability. *Phys. Rev.* E **61**, 6546–6562.

Nie, X., Qian, Y., Doolen, G. D. & Chen, S. 1998 Lattice Boltzmann simulation of the two-dimensional Rayleigh-Taylor instability. *Phys. Rev.* E **58**, 6861–6864.

Papanastasiou, T. C. 1987 Flows of materials with yield. *J. of Rheol.* **31**, 385–404.

Bisher erschienene Berichte des Fraunhofer ITWM

Die PDF-Files der folgenden Berichte finden Sie unter:
www.itwm.fhg.de/zentral/berichte.html

1. D. Hietel, K. Steiner, J. Struckmeier

A Finite - Volume Particle Method for Compressible Flows

We derive a new class of particle methods for conservation laws, which are based on numerical flux functions to model the interactions between moving particles. The derivation is similar to that of classical Finite-Volume methods; except that the fixed grid structure in the Finite-Volume method is substituted by so-called mass packets of particles. We give some numerical results on a shock wave solution for Burgers equation as well as the well-known one-dimensional shock tube problem.
(19 S., 1998)

2. M. Feldmann, S. Seibold

Damage Diagnosis of Rotors: Application of Hilbert Transform and Multi-Hypothesis Testing

In this paper, a combined approach to damage diagnosis of rotors is proposed. The intention is to employ signal-based as well as model-based procedures for an improved detection of size and location of the damage. In a first step, Hilbert transform signal processing techniques allow for a computation of the signal envelope and the instantaneous frequency, so that various types of non-linearities due to a damage may be identified and classified based on measured response data. In a second step, a multi-hypothesis bank of Kalman Filters is employed for the detection of the size and location of the damage based on the information of the type of damage provided by the results of the Hilbert transform.
Keywords:
Hilbert transform, damage diagnosis, Kalman filtering, non-linear dynamics
(23 S., 1998)

3. Y. Ben-Haim, S. Seibold

Robust Reliability of Diagnostic Multi-Hypothesis Algorithms: Application to Rotating Machinery

Damage diagnosis based on a bank of Kalman filters, each one conditioned on a specific hypothesized system condition, is a well recognized and powerful diagnostic tool. This multi-hypothesis approach can be applied to a wide range of damage conditions. In this paper, we will focus on the diagnosis of cracks in rotating machinery. The question we address is: how to optimize the multi-hypothesis algorithm with respect to the uncertainty of the spatial form and location of cracks and their resulting dynamic effects. First, we formulate a measure of the reliability of the diagnostic algorithm, and then we discuss modifications of the diagnostic algorithm for the maximization of the reliability. The reliability of a diagnostic algorithm is measured by the amount of uncertainty consistent with no-failure of the diagnosis. Uncertainty is quantitatively represented with convex models.
Keywords:
Robust reliability, convex models, Kalman filtering, multi-hypothesis diagnosis, rotating machinery, crack diagnosis
(24 S., 1998)

4. F.-Th. Lentes, N. Siedow

Three-dimensional Radiative Heat Transfer in Glass Cooling Processes

For the numerical simulation of 3D radiative heat transfer in glasses and glass melts, practically applicable mathematical methods are needed to handle such problems optimal using workstation class computers. Since the exact solution would require super-computer capabilities we concentrate on approximate solutions with a high degree of accuracy. The following approaches are studied: 3D diffusion approximations and 3D ray-tracing methods.
(23 S., 1998)

5. A. Klar, R. Wegener

A hierarchy of models for multilane vehicular traffic
Part I: Modeling

In the present paper multilane models for vehicular traffic are considered. A microscopic multilane model based on reaction thresholds is developed. Based on this model an Enskog like kinetic model is developed. In particular, care is taken to incorporate the correlations between the vehicles. From the kinetic model a fluid dynamic model is derived. The macroscopic coefficients are deduced from the underlying kinetic model. Numerical simulations are presented for all three levels of description in [10]. Moreover, a comparison of the results is given there.
(23 S., 1998)

Part II: Numerical and stochastic investigations

In this paper the work presented in [6] is continued. The present paper contains detailed numerical investigations of the models developed there. A numerical method to treat the kinetic equations obtained in [6] are presented and results of the simulations are shown. Moreover, the stochastic correlation model used in [6] is described and investigated in more detail.
(17 S., 1998)

6. A. Klar, N. Siedow

Boundary Layers and Domain Decomposition for Radiative Heat Transfer and Diffusion Equations: Applications to Glass Manufacturing Processes

In this paper domain decomposition methods for radiative transfer problems including conductive heat transfer are treated. The paper focuses on semi-transparent materials, like glass, and the associated conditions at the interface between the materials. Using asymptotic analysis we derive conditions for the coupling of the radiative transfer equations and a diffusion approximation. Several test cases are treated and a problem appearing in glass manufacturing processes is computed. The results clearly show the advantages of a domain decomposition approach. Accuracy equivalent to the solution of the global radiative transfer solution is achieved, whereas computation time is strongly reduced.
(24 S., 1998)

7. I. Choquet

Heterogeneous catalysis modelling and numerical simulation in rarified gas flows Part I: Coverage locally at equilibrium

A new approach is proposed to model and simulate numerically heterogeneous catalysis in rarefied gas flows. It is developed to satisfy all together the following points:
1) describe the gas phase at the microscopic scale, as required in rarefied flows,
2) describe the wall at the macroscopic scale, to avoid prohibitive computational costs and consider not only crystalline but also amorphous surfaces,
3) reproduce on average macroscopic laws correlated with experimental results and
4) derive analytic models in a systematic and exact way.
The problem is stated in the general framework of a non static flow in the vicinity of a catalytic and non porous surface (without aging). It is shown that the exact and systematic resolution method based on the Laplace transform, introduced previously by the author to model collisions in the gas phase, can be extended to the present problem. The proposed approach is applied to the modelling of the Eley-Rideal and Langmuir-Hinshelwood recombinations, assuming that the coverage is locally at equilibrium. The models are developed considering one atomic species and extended to the general case of several atomic species. Numerical calculations show that the models derived in this way reproduce with accuracy behaviors observed experimentally.
(24 S., 1998)

8. J. Ohser, B. Steinbach, C. Lang

Efficient Texture Analysis of Binary Images

A new method of determining some characteristics of binary images is proposed based on a special linear filtering. This technique enables the estimation of the area fraction, the specific line length, and the specific integral of curvature. Furthermore, the specific length of the total projection is obtained, which gives detailed information about the texture of the image. The influence of lateral and directional resolution depending on the size of the applied filter mask is discussed in detail. The technique includes a method of increasing directional resolution for texture analysis while keeping lateral resolution as high as possible.
(17 S., 1998)

9. J. Orlik

Homogenization for viscoelasticity of the integral type with aging and shrinkage

A multi-phase composite with periodic distributed inclusions with a smooth boundary is considered in this contribution. The composite component materials are supposed to be linear viscoelastic and aging (of the non-convolution integral type, for which the Laplace transform with respect to time is not effectively applicable) and are subjected to isotropic shrinkage. The free shrinkage deformation can be considered as a fictitious temperature deformation in the behavior law. The procedure presented in this paper proposes a way to determine average (effective homogenized) viscoelastic and shrinkage (temperature) composite properties and the homogenized stress-field from known properties of the

components. This is done by the extension of the asymptotic homogenization technique known for pure elastic non-homogeneous bodies to the non-homogeneous thermo-viscoelasticity of the integral non-convolution type. Up to now, the homogenization theory has not covered viscoelasticity of the integral type.
Sanchez-Palencia (1980), Francfort & Suquet (1987) (see [2], [9]) have considered homogenization for viscoelasticity of the differential form and only up to the first derivative order. The integral-modeled viscoelasticity is more general then the differential one and includes almost all known differential models. The homogenization procedure is based on the construction of an asymptotic solution with respect to a period of the composite structure. This reduces the original problem to some auxiliary boundary value problems of elasticity and viscoelasticity on the unit periodic cell, of the same type as the original non-homogeneous problem. The existence and uniqueness results for such problems were obtained for kernels satisfying some constrain conditions. This is done by the extension of the Volterra integral operator theory to the Volterra operators with respect to the time, whose 1 kernels are space linear operators for any fixed time variables. Some ideas of such approach were proposed in [11] and [12], where the Volterra operators with kernels depending additionally on parameter were considered. This manuscript delivers results of the same nature for the case of the space-operator kernels.
(20 S., 1998)

10. J. Mohring

Helmholtz Resonators with Large Aperture

The lowest resonant frequency of a cavity resonator is usually approximated by the classical Helmholtz formula. However, if the opening is rather large and the front wall is narrow this formula is no longer valid. Here we present a correction which is of third order in the ratio of the diameters of aperture and cavity. In addition to the high accuracy it allows to estimate the damping due to radiation. The result is found by applying the method of matched asymptotic expansions. The correction contains form factors describing the shapes of opening and cavity. They are computed for a number of standard geometries. Results are compared with numerical computations.
(21 S., 1998)

11. H. W. Hamacher, A. Schöbel

On Center Cycles in Grid Graphs

Finding "good" cycles in graphs is a problem of great interest in graph theory as well as in locational analysis. We show that the center and median problems are NP hard in general graphs. This result holds both for the variable cardinality case (i.e. all cycles of the graph are considered) and the fixed cardinality case (i.e. only cycles with a given cardinality p are feasible). Hence it is of interest to investigate special cases where the problem is solvable in polynomial time.
In grid graphs, the variable cardinality case is, for instance, trivially solvable if the shape of the cycle can be chosen freely.
If the shape is fixed to be a rectangle one can analyze rectangles in grid graphs with, in sequence, fixed dimension, fixed cardinality, and variable cardinality. In all cases a complete characterization of the optimal cycles and closed form expressions of the optimal objective values are given, yielding polynomial time algorithms for all cases of center rectangle problems.
Finally, it is shown that center cycles can be chosen as rectangles for small cardinalities such that the center cycle problem in grid graphs is in these cases completely solved.
(15 S., 1998)

12. H. W. Hamacher, K.-H. Küfer

Inverse radiation therapy planning - a multiple objective optimisation approach

For some decades radiation therapy has been proved successful in cancer treatment. It is the major task of clinical radiation treatment planning to realize on the one hand a high level dose of radiation in the cancer tissue in order to obtain maximum tumor control. On the other hand it is obvious that it is absolutely necessary to keep in the tissue outside the tumor, particularly in organs at risk, the unavoidable radiation as low as possible.
No doubt, these two objectives of treatment planning - high level dose in the tumor, low radiation outside the tumor - have a basically contradictory nature. Therefore, it is no surprise that inverse mathematical models with dose distribution bounds tend to be infeasible in most cases. Thus, there is need for approximations compromising between overdosing the organs at risk and underdosing the target volume.
Differing from the currently used time consuming iterative approach, which measures deviation from an ideal (non-achievable) treatment plan using recursively trial-and-error weights for the organs of interest, we go a new way trying to avoid a priori weight choices and consider the treatment planning problem as a multiple objective linear programming problem: with each organ of interest, target tissue as well as organs at risk, we associate an objective function measuring the maximal deviation from the prescribed doses.
We build up a data base of relatively few efficient solutions representing and approximating the variety of Pareto solutions of the multiple objective linear programming problem. This data base can be easily scanned by physicians looking for an adequate treatment plan with the aid of an appropriate online tool.
(14 S., 1999)

13. C. Lang, J. Ohser, R. Hilfer

On the Analysis of Spatial Binary Images

This paper deals with the characterization of microscopically heterogeneous, but macroscopically homogeneous spatial structures. A new method is presented which is strictly based on integral-geometric formulae such as Crofton's intersection formulae and Hadwiger's recursive definition of the Euler number. The corresponding algorithms have clear advantages over other techniques. As an example of application we consider the analysis of spatial digital images produced by means of Computer Assisted Tomography.
(20 S., 1999)

14. M. Junk

On the Construction of Discrete Equilibrium Distributions for Kinetic Schemes

A general approach to the construction of discrete equilibrium distributions is presented. Such distribution functions can be used to set up Kinetic Schemes as well as Lattice Boltzmann methods. The general principles are also applied to the construction of Chapman Enskog distributions which are used in Kinetic Schemes for compressible Navier-Stokes equations.
(24 S., 1999)

15. M. Junk, S. V. Raghurame Rao

A new discrete velocity method for Navier-Stokes equations

The relation between the Lattice Boltzmann Method, which has recently become popular, and the Kinetic Schemes, which are routinely used in Computational Fluid Dynamics, is explored. A new discrete velocity model for the numerical solution of Navier-Stokes equations for incompressible fluid flow is presented by combining both the approaches. The new scheme can be interpreted as a pseudo-compressibility method and, for a particular choice of parameters, this interpretation carries over to the Lattice Boltzmann Method.
(20 S., 1999)

16. H. Neunzert

Mathematics as a Key to Key Technologies

The main part of this paper will consist of examples, how mathematics really helps to solve industrial problems; these examples are taken from our Institute for Industrial Mathematics, from research in the Technomathematics group at my university, but also from ECMI groups and a company called TecMath, which originated 10 years ago from my university group and has already a very successful history.
(39 S. (vier PDF-Files), 1999)

17. J. Ohser, K. Sandau

Considerations about the Estimation of the Size Distribution in Wicksell's Corpuscle Problem

Wicksell's corpuscle problem deals with the estimation of the size distribution of a population of particles, all having the same shape, using a lower dimensional sampling probe. This problem was originary formulated for particle systems occurring in life sciences but its solution is of actual and increasing interest in materials science. From a mathematical point of view, Wicksell's problem is an inverse problem where the interesting size distribution is the unknown part of a Volterra equation. The problem is often regarded ill-posed, because the structure of the integrand implies unstable numerical solutions. The accuracy of the numerical solutions is considered here using the condition number, which allows to compare different numerical methods with different (equidistant) class sizes and which indicates, as one result, that a finite section thickness of the probe reduces the numerical problems. Furthermore, the relative error of estimation is computed which can be split into two parts. One part consists of the relative discretization error that increases for increasing class size, and the second part is related to the relative statistical error which increases with decreasing class size. For both parts, upper bounds can be given and the sum of them indicates an optimal class width depending on some specific constants.
(18 S., 1999)

18. E. Carrizosa, H. W. Hamacher, R. Klein, S. Nickel

Solving nonconvex planar location problems by finite dominating sets

It is well-known that some of the classical location problems with polyhedral gauges can be solved in polynomial time by finding a finite dominating set, i. e. a finite set of candidates guaranteed to contain at least one optimal location.
In this paper it is first established that this result holds for a much larger class of problems than currently considered in the literature. The model for which this result can be proven includes, for instance, location problems with attraction and repulsion, and location-allocation problems. Next, it is shown that the approximation of general gauges by polyhedral ones in the objective function of our general model can be analyzed with regard to the subsequent error in the optimal objective value. For the approximation problem two different approaches are described, the sandwich procedure and the greedy algorithm. Both of these approaches lead - for fixed epsilon - to polynomial approximation algorithms with accuracy epsilon for solving the general model considered in this paper.
Keywords:
Continuous Location, Polyhedral Gauges, Finite Dominating Sets, Approximation, Sandwich Algorithm, Greedy Algorithm
(19 S., 2000)

19. A. Becker

A Review on Image Distortion Measures

Within this paper we review image distortion measures. A distortion measure is a criterion that assigns a "quality number" to an image. We distinguish between mathematical distortion measures and those distortion measures in-cooperating a priori knowledge about the imaging devices (e. g. satellite images), image processing algorithms or the human physiology. We will consider representative examples of different kinds of distortion measures and are going to discuss them.
Keywords:
Distortion measure, human visual system
(26 S., 2000)

20. H. W. Hamacher, M. Labbé, S. Nickel, T. Sonneborn

Polyhedral Properties of the Uncapacit*ated Multiple Allocation Hub Location Problem*

We examine the feasibility polyhedron of the uncapacitated hub location problem (UHL) with multiple allocation, which has applications in the fields of air passenger and cargo transportation, telecommunication and postal delivery services. In particular we determine the dimension and derive some classes of facets of this polyhedron. We develop some general rules about lifting facets from the uncapacitated facility location (UFL) for UHL and projecting facets from UHL to UFL. By applying these rules we get a new class of facets for UHL which dominates the inequalities in the original formulation. Thus we get a new formulation of UHL whose constraints are all facet–defining. We show its superior computational performance by benchmarking it on a well known data set.
Keywords:
integer programming, hub location, facility location, valid inequalities, facets, branch and cut
(21 S., 2000)

21. H. W. Hamacher, A. Schöbel

Design of Zone Tariff Systems in Public Transportation

Given a public transportation system represented by its stops and direct connections between stops, we consider two problems dealing with the prices for the customers: The fare problem in which subsets of stops are already aggregated to zones and "good" tariffs have to be found in the existing zone system. Closed form solutions for the fare problem are presented for three objective functions. In the zone problem the design of the zones is part of the problem. This problem is NP hard and we therefore propose three heuristics which prove to be very successful in the redesign of one of Germany's transportation systems.
(30 S., 2001)

22. D. Hietel, M. Junk, R. Keck, D. Teleaga:

The Finite-Volume-Particle Method for Conservation Laws

In the Finite-Volume-Particle Method (FVPM), the weak formulation of a hyperbolic conservation law is discretized by restricting it to a discrete set of test functions. In contrast to the usual Finite-Volume approach, the test functions are not taken as characteristic functions of the control volumes in a spatial grid, but are chosen from a partition of unity with smooth and overlapping partition functions (the particles), which can even move along prescribed velocity fields. The information exchange between particles is based on standard numerical flux functions. Geometrical information, similar to the surface area of the cell faces in the Finite-Volume Method and the corresponding normal directions are given as integral quantities of the partition functions.
After a brief derivation of the Finite-Volume-Particle Method, this work focuses on the role of the geometric coefficients in the scheme.
(16 S., 2001)

23. T. Bender, H. Hennes, J. Kalcsics, M. T. Melo, S. Nickel

Location Software and Interface with GIS and Supply Chain Management

The objective of this paper is to bridge the gap between location theory and practice. To meet this objective focus is given to the development of software capable of addressing the different needs of a wide group of users. There is a very active community on location theory encompassing many research fields such as operations research, computer science, mathematics, engineering, geography, economics and marketing. As a result, people working on facility location problems have a very diverse background and also different needs regarding the software to solve these problems. For those interested in non-commercial applications (e. g. students and researchers), the library of location algorithms (LoLA can be of considerable assistance. LoLA contains a collection of efficient algorithms for solving planar, network and discrete facility location problems. In this paper, a detailed description of the functionality of LoLA is presented. In the fields of geography and marketing, for instance, solving facility location problems requires using large amounts of demographic data. Hence, members of these groups (e. g. urban planners and sales managers) often work with geographical information too s. To address the specific needs of these users, LoLA was inked to a geographical information system (GIS) and the details of the combined functionality are described in the paper. Finally, there is a wide group of practitioners who need to solve large problems and require special purpose software with a good data interface. Many of such users can be found, for example, in the area of supply chain management (SCM). Logistics activities involved in strategic SCM include, among others, facility location planning. In this paper, the development of a commercial location software tool is also described. The too is embedded in the Advanced Planner and Optimizer SCM software developed by SAP AG, Walldorf, Germany. The paper ends with some conclusions and an outlook to future activities.
Keywords:
facility location, software development, geographical information systems, supply chain management.
(48 S., 2001)

24. H. W. Hamacher, S. A. Tjandra

Mathematical Modelling of Evacuation Problems: A State of Art

This paper details models and algorithms which can be applied to evacuation problems. While it concentrates on building evacuation many of the results are applicable also to regional evacuation. All models consider the time as main parameter, where the travel time between components of the building is part of the input and the overall evacuation time is the output. The paper distinguishes between macroscopic and microscopic evacuation models both of which are able to capture the evacuees' movement over time.
Macroscopic models are mainly used to produce good lower bounds for the evacuation time and do not consider any individual behavior during the emergency situation. These bounds can be used to analyze existing buildings or help in the design phase of planning a building. Macroscopic approaches which are based on dynamic network flow models (minimum cost dynamic flow, maximum dynamic flow, universal maximum flow, quickest path and quickest flow) are described. A special feature of the presented approach is the fact, that travel times of evacuees are not restricted to be constant, but may be density dependent. Using multicriteria optimization priority regions and blockage due to fire or smoke may be considered. It is shown how the modelling can be done using time parameter either as discrete or continuous parameter.
Microscopic models are able to model the individual evacuee's characteristics and the interaction among evacuees which influence their movement. Due to the corresponding huge amount of data one uses simulation approaches. Some probabilistic laws for individual evacuee's movement are presented. Moreover ideas to model the evacuee's movement using cellular automata (CA) and resulting software are presented.
In this paper we will focus on macroscopic models and only summarize some of the results of the microscopic approach. While most of the results are applicable to general evacuation situations, we concentrate on building evacuation.
(44 S., 2001)

25. J. Kuhnert, S. Tiwari

Grid free method for solving the Poisson equation

A Grid free method for solving the Poisson equation is presented. This is an iterative method. The method is based on the weighted least squares approximation in which the Poisson equation is enforced to be satisfied in every iterations. The boundary conditions can also be enforced in the iteration process. This is a local approximation procedure. The Dirichlet, Neumann and mixed boundary value problems on a unit square are presented and the analytical solutions are compared with the exact solutions. Both solutions matched perfectly.
Keywords:
Poisson equation, Least squares method, Grid free method
(19 S., 2001)

26. T. Götz, H. Rave, D. Reinel-Bitzer, K. Steiner, H. Tiemeier

Simulation of the fiber spinning process

To simulate the influence of process parameters to the melt spinning process a fiber model is used and coupled with CFD calculations of the quench air flow. In the fiber model energy, momentum and mass balance are solved for the polymer mass flow. To calculate the quench air the Lattice Boltzmann method is used. Simulations and experiments for different process parameters and hole configurations are compared and show a good agreement.
Keywords:
Melt spinning, fiber model, Lattice Boltzmann, CFD
(19 S., 2001)

27. A. Zemitis

On interaction of a liquid film with an obstacle

In this paper mathematical models for liquid films generated by impinging jets are discussed. Attention is stressed to the interaction of the liquid film with some obstacle. S. G. Taylor [Proc. R. Soc. London Ser. A 253, 313 (1959)] found that the liquid film generated by impinging jets is very sensitive to properties of the wire which was used as an obstacle. The aim of this presentation is to propose a modification of the Taylor's model, which allows to simulate the film shape in cases, when the angle between jets is different from 180°. Numerical results obtained by discussed models give two different shapes of the liquid film similar as in Taylors experiments. These two shapes depend on the regime: either droplets are produced close to the obstacle or not. The difference between two regimes becomes larger if the angle between jets decreases. Existence of such two regimes can be very essential for some applications of impinging jets, if the generated liquid film can have a contact with obstacles.
Keywords:
impinging jets, liquid film, models, numerical solution, shape
(22 S., 2001)

28. I. Ginzburg, K. Steiner

Free surface lattice-Boltzmann method to model the filling of expanding cavities by Bingham Fluids

The filling process of viscoplastic metal alloys and plastics in expanding cavities is modelled using the lattice Boltzmann method in two and three dimensions. These models combine the regularized Bingham model for viscoplastic with a free-interface algorithm. The latter is based on a modified immiscible lattice Boltzmann model in which one species is the fluid and the other one is considered as vacuum. The boundary conditions at the curved liquid-vacuum interface are met without any geometrical front reconstruction from a first-order Chapman-Enskog expansion. The numerical results obtained with these models are found in good agreement with available theoretical and numerical analysis.
Keywords:
Generalized LBE, free-surface phenomena, interface boundary conditions, filling processes, Bingham viscoplastic model, regularized models
(22 S., 2001)